Matrix algorithm for solving Schrödinger equations with position-dependent mass or complex optical potentials

Johann Förster, Alejandro Saenz and Ulli Wolff
Institut für Physik, Humboldt-Universität zu Berlin, Newtonstr. 15, 12489 Berlin, Germany

We represent low dimensional quantum mechanical Hamiltonians by moderately sized finite matrices that reproduce the lowest O(10) boundstate energies and wave functions to machine precision. The method extends also to Hamiltonians that are neither Hermitian nor PT symmetric and thus allows to investigate whether or not the spectra in such cases are still real. Furthermore, the approach is especially useful for problems in which a position-dependent mass is adopted, for example in effective-mass models in solid-state physics or in the approximate treatment of coupled nuclear motion in molecular physics or quantum chemistry. The performance of the algorithm is demonstrated by considering the inversion motion of different isotopes of ammonia molecules within a position-dependent mass model and some other examples of one- and two-dimensional Hamiltonians that allow for the comparison to analytical or numerical results in the literature.

I. INTRODUCTION

In a number of cases complex systems can be treated in a simplified manner, if a position-dependent mass is introduced. One prominent example is the concept of an effective electron mass in solid-state physics where position-dependent masses provide a way to obtain corrections to the simplest approach in which a constant effective mass is used (see, e. g., [1] and references therein). As a consequence, Schrödinger equations with a position-dependent mass have been considered in various contexts, for example to study electronic properties of semiconductors [2], He clusters [3], or super-lattice band structures [4].

Also in molecular physics or theoretical chemistry position-dependent masses can occur, if high-dimensional nuclear motion is described using a lower dimensional effective Hamiltonian. A rather well known example is the theoretical description of the inversion motion (umbrella mode) in ammonia molecules (NH_3) in which the nitrogen atom is moving from one side of the plane formed by the three hydrogen atoms to the other. In fact, this involves a collective motion, since the hydrogen-nitrogen bonds change their lengths while the nitrogen atom moves. This is thus an example of strongly coupled vibrational modes, in this case of the symmetric bending and stretching modes. While the main physics of this motion can be captured by an effective one-dimensional double-well potential, an improved approximation is achieved by introducing a position-dependent mass while still maintaining a one-dimensional treatment. The inversion motion of ammonia and its one-dimensional model has been studied extensively in several papers, e. g., in [5–8], and has been exploited for the ammonia maser [9]. Especially Aquino *et al*. [7] obtained very accurate results in comparison to experiment by reducing the two-dimensional problem to a one-dimensional problem with a position-dependent reduced mass. Note that this ansatz is deduced from classical arguments and thus leads to quantum mechanical operator ordering ambiguities, since it is not clear anymore how to order the operators in the kinetic term $p^2/2m$. The accurate and efficient solution of a Schrödinger equation with a position-dependent mass is non-trivial and various efforts were made even recently to find analytical or numerical solutions, e. g., in [1, 10, 11].

In this work a matrix method is introduced that determines efficiently and accurately the bound states of Schrödinger equations with a position-dependent mass. The algorithm is very flexible and allows to consider different symmetrized or non-symmetrized forms of the kinetic-energy operator. Furthermore, also non-Hermitian Hamiltonians can be treated, including complex ones. Non-Hermitian PT-symmetric Hamiltonians have recently stirred some interest [12, 13] in connection with the question under which circumstances the spectrum may still remain real. In addition to that, non-Hermitian Hamiltonians (also without PT-symmetry) occur for example in the context of complex optical potentials (see, e. g., [14, 15]).

After a brief discussion of Hamiltonians with a position-dependent mass or PT symmetry in Sec. II the method is presented in Sec. III. In Sec. IV the performance of the method is discussed for a number of examples. This includes a study of the inversion mode of NH_3 (Sec. IV A) and ND_3 (Sec. IV B), the Morse potential (Sec. IV D), a harmonic oscillator with position-dependent mass (Sec. IV E), and examples of PT-symmetric and non-symmetric non-Hermitian Hamiltonians (Sec. IV F). We also use the example in Sec. IV A to discuss the convergence properties of the method (Sec. IV C). In addition to these one-dimensional examples, we discuss the application of the algorithm to the two-dimensional Henon-Heiles system (Sec. IV G).

II. POSITION-DEPENDENT MASS AND PT-SYMMETRIC SCHRÖDINGER EQUATIONS

We want to replace $m \to m(\hat{x})$ in one-dimensional quantum systems and, therefore, investigate various ways to order the operators in the kinetic-energy terms. A whole class of Hermitian Hamiltonians with position-

dependent mass is given by the von Roos Hamiltonians [16],

$$\hat{\mathrm{H}} = \frac{1}{4}\left(\hat{\mathrm{m}}^{\alpha}\hat{\mathrm{p}}\,\hat{\mathrm{m}}^{\beta}\hat{\mathrm{p}}\hat{\mathrm{m}}^{\gamma} + \hat{\mathrm{m}}^{\gamma}\hat{\mathrm{p}}\,\hat{\mathrm{m}}^{\beta}\hat{\mathrm{p}}\hat{\mathrm{m}}^{\alpha}\right) + V(\hat{\mathrm{x}}) \tag{1}$$

with

$$\alpha + \beta + \gamma = -1 \tag{2}$$

and $\hat{\mathrm{m}} = m(\hat{\mathrm{x}})$ with the usual canonical operators $\hat{\mathrm{p}}$ and $\hat{\mathrm{x}}$. The choice $\alpha = \gamma = 0$, $\beta = -1$ leads to

$$\hat{\mathrm{H}} = \frac{1}{2}\hat{\mathrm{p}}\,\frac{1}{\hat{\mathrm{m}}}\,\hat{\mathrm{p}} + V(\hat{\mathrm{x}}), \tag{3}$$

while with $\alpha = -1$, $\beta = \gamma = 0$ one finds

$$\hat{\mathrm{H}} = \frac{1}{4}\left(\frac{1}{\hat{\mathrm{m}}}\,\hat{\mathrm{p}}^2 + \hat{\mathrm{p}}^2\,\frac{1}{\hat{\mathrm{m}}}\right) + V(\hat{\mathrm{x}}). \tag{4}$$

While there is no *a priory* reason to favor any of the Hermitian Hamiltonians, for example a specific choice of α, β, and γ, non-Hermitian Hamiltonians are often rejected for general reasons, since they can possess complex eigenvalues. However, in standard quantum mechanics *closed* systems are described by Hermitian Hamiltonians and real eigenvalue spectra. (Note that non-Hermitian Hamiltonians occur, e. g., in the approximate description of open systems with optical potentials.) Regarding the reality of the spectrum, non-Hermitian PT-symmetric Hamiltonians form a special class as discussed in [12, 13]. Therefore, they are of special interest for possible extensions of standard quantum mechanics. Note, however, that these extensions often also involve a complex potential instead of a position-dependent mass. For the NH_3 molecule the position-dependent reduced mass $\mu(x)$ in [7] was derived within classical mechanics and then translated into quantum mechanics in the form

$$\hat{\mathrm{H}} = \frac{1}{2\hat{\mathrm{m}}}\,\hat{\mathrm{p}}^2 + V(\hat{\mathrm{x}}) \tag{5}$$

which is non-Hermitian, but convenient for computation. The advantage of Eq. (5) is that no first derivative of the wavefunction occurs. This simplifies the numerical solution with standard approaches. For example, the Numerov-Cooley method [17, 18] can be adopted as was done in [6]. Another possible non-Hermitian choice is

$$\hat{\mathrm{H}} = \hat{\mathrm{p}}^2\,\frac{1}{2\hat{\mathrm{m}}} + V(\hat{\mathrm{x}}). \tag{6}$$

(Note if both the potential V and the mass m possess inversion symmetry, $V(x) = V(-x)$ and $m(x) = m(-x)$, as is the case for ammonia, then the Hamiltonians in Eqs. (5) and (6) are P and T symmetric.)

It is important to not only have an efficient and reliable solver for one version of the Hamiltonian, but to be able to compare the results of different versions. Ideally, the results agree sufficiently well and thus the question of the proper form becomes practically inessential for the attempted approximation level. A strong variation of the results with the chosen form of the Hamiltonian, on the other hand, is a clear warning signal. Since non-Hermitian and (for example for $V(x) \neq V(-x)$) in principle even PT non-symmetric Hamiltonians can be obtained for some versions of the Hamiltonians with a position-dependent mass, it is also of interest to have a solver that can handle these cases and that detects possible non-vanishing imaginary components of the eigenvalues. This is, in fact, also an important issue in the general context of PT-symmetric Hamiltonians (or other proposals for extensions of standard quantum mechanics) without position-dependent masses. Since in the majority of cases physically relevant Hamiltonians do not possess analytical solutions, it is important to numerically check whether the eigenvalue spectrum is purely real or not. The algorithm presented below provides a promising solution to this type of problems. Position-dependent masses are easily handled, even for different formulations of the kinetic-energy operator. Furthermore, a number of bound states are obtained simultaneously within a single calculation. Finally, the algorithm can equally well be applied to complex Hamiltonians and thus also to non-Hermitian Hamiltonians with either purely real or partly complex eigenvalues.

III. THE MATRIX ALGORITHM

The technique to investigate simple quantum systems reviewed below has been taught by one of us (U. W.) in the computational physics courses at Humboldt university since 2006. It has also recently been used for supersymmetric quantum mechanics in [19]. The basis is the so-called SLAC derivative that was proposed for lattice fermions in [20]. While it had to be discarded for four dimensional quantum field theory due to incompatibilities with ultraviolet renormalization [21] no such problems seem to hamper the present quantum mechanical applications.

We define a one-dimensional position space lattice consisting of an odd number of $N = 2M + 1$ points

$$\{x_1, x_2, \ldots, x_N\} = \{-Ma, -(M-1)a, \ldots, -a, 0, a, \ldots, Ma\}. \tag{7}$$

that are equidistantly spaced with the lattice spacing a and lie symmetrically around the origin. Wave 'functions' in the Schrödinger representation of quantum mechanics are restricted to this space

$$\Psi(x) \equiv \begin{pmatrix} \Psi(x_1) \\ \Psi(x_2) \\ \vdots \\ \Psi(x_N) \end{pmatrix}, \tag{8}$$

and thus the Hilbert space is approximated by $\mathbb{C}^N$. Intuitively, a bound state that is centered around the origin,

can be represented well in this framework, if its size is much smaller than $L = Na$ such that the sites $\pm Ma$ are deeply in the classically forbidden region. Moreover a must be small enough to allow for a good resolution of structures in the wave function. For example, for a simple harmonic oscillator of mass m and frequency ω these conditions amount to $a \ll \sqrt{\hbar/(m\omega)} \ll L$.

Linear operators must become finite matrices now. Functions of the position operator like the potential $V(\hat{\mathrm{x}})$ trivially translate into diagonal matrices

$$(V\Psi)(x) \equiv \begin{pmatrix} V(x_1)\Psi(x_1) \\ V(x_2)\Psi(x_2) \\ \vdots \\ V(x_N)\Psi(x_N) \end{pmatrix}. \tag{9}$$

To also implement a canonically conjugate momentum operator $\hat{\mathrm{p}}$ that has to mimic the derivative, we need to impose boundary conditions which we take periodic with period L. Note that this also implies a periodic extension of the diagonal elements of the position operator. This means that odd powers of $\hat{\mathrm{x}}$ create jumps at odd-integer multiples of $L/2$, in particular at $\pm Ma$, which will, however, be seen to cause no problems in our applications here. The first idea that comes to mind now is to represent $\hat{\mathrm{p}}^2$ by a difference operator over three (or more) sites. This would clearly inflict leading discretization errors that are powers of a^2. We found that a better precision is obtained by Fourier transforming, then using a diagonal operator for $\hat{\mathrm{p}}^2$ analogous to the one in discrete position space and then transforming back. This results in a nonlocal matrix representation in position space that couples *all* sites given by

$$(f(\hat{\mathrm{p}}))_{ik} = \frac{1}{N}\sum_p f(p)\exp[ip(x_i - x_k)]. \tag{10}$$

where the p-sum runs over the values

$$\{p_1, p_2, \ldots, p_N\} = \left\{-M\frac{2\pi}{L}, -(M-1)\frac{2\pi}{L}, \ldots, M\frac{2\pi}{L}\right\} \tag{11}$$

and periodicity under shifts of p by $\pm 2\pi/a$ holds.

A multiplication of a wave function with the above matrix may be decomposed into two steps. First we compute

$$\tilde{\Psi}(p) = a\sum_{k=1}^{N}\exp[-ipx_k]\Psi(x_k) \to \int_{-L/2}^{L/2} dy \exp[-ipy]\Psi(y) \tag{12}$$

where the continuum limit $a \to 0$ at fixed L is indicated (for a continuously defined Ψ). In the second step we form

$$(f(\hat{\mathrm{p}})\Psi)(x) = \frac{1}{L}\sum_p f(p)\exp[ipx]\tilde{\Psi}(p). \tag{13}$$

Here x can in any case assume continuous values and inside f obviously p is equivalent to $-id/dx$. The p-sum becomes infinite in the continuum limit.

Returning to finite a and L the formula (setting $j = i - k$)

$$\begin{aligned}(\exp[i\alpha\hat{\mathrm{p}}])_{ik} &= \frac{1}{N}\sum_p \exp[ip(\alpha + x_i - x_k)] \\ &= \frac{(-1)^j}{N}\,\frac{\sin(\pi\alpha/a)}{\sin(\pi(\alpha + ja)/L)}\end{aligned} \tag{14}$$

which holds for general α, allows for the explicit computation of matrix elements of powers of $\hat{\mathrm{p}}$. Comparing powers in α we find for example

$$(\hat{\mathrm{p}})_{ik} = \begin{cases} 0 & \text{for} \quad j = 0 \bmod N \\ \frac{\pi}{iL}\frac{(-1)^j}{\sin(\pi j/N)} & \text{else} \end{cases}, \tag{15}$$

$$(\hat{\mathrm{p}}^2)_{ik} = \begin{cases} \frac{\pi^2}{3a^2}(1 - a^2/L^2) & \text{for} \quad j = 0 \bmod N \\ \frac{2\pi^2}{L^2}\frac{(-1)^j\cos(\pi j/N)}{\sin^2(\pi j/N)} & \text{else} \end{cases} \tag{16}$$

Equivalently, we may of course also take matrix powers of $(\hat{\mathrm{p}})_{ik}$.

To find the eigenvalues of the Schrödinger equation we now construct the matrix representation of $\hat{\mathrm{H}}$ and diagonalize this matrix to find eigenenergies E_n and eigenfunctions Ψ_n of the system. Clearly, the width L and the number of points N should be sufficiently large to obtain converged results and only a certain number of low-lying energies E_n can be expected to be reliable for any fixed N and L.

To diagonalize the matrix, we implement the matrix in MATLAB [22] and employ the routine *eig* which determines eigenvalues and eigenvectors of a matrix (also for non-Hermitian matrices). A simple MATLAB code to construct the matrix representation of the Hamiltonian for the first application discussed in Sec. IV A (ammonia inversion) is explicitly given in the appendix.

As will be discussed in Sec. IV C, the matrix algorithm has a very fast convergence behavior such that around 100 points are usually sufficient. Therefore, also higher dimensional problems with for example about $N_x \times N_y = \mathrm{O}(10^4)$ points in two dimensions are within reach on present-day computers. In that case we discretize each direction as before and obtain a rectangle filled with sites

$$\vec{r}_I = (x_{i_1}, y_{i_2}), \quad i_1 = 1, \ldots, N_x, \quad i_2 = 1, \ldots, N_y \tag{17}$$

with the unique compound index

$$I = i_1 + (i_2 - 1)N_x = 1, \ldots, N_x N_y. \tag{18}$$

Operators are embedded in the tensor product state space. The position operators become for example

$$(\hat{\mathrm{x}})_{IK} = x_{i_1}\delta_{i_1k_1}\delta_{i_2k_2}, \quad (\hat{y})_{IK} = y_{i_2}\delta_{i_1k_1}\delta_{i_2k_2}. \tag{19}$$

Similarly $\hat{\mathrm{p}}_x^2$ leads to a matrix

$$(\hat{\mathrm{p}}_x^2)_{IK} = (\hat{\mathrm{p}}^2)_{i_1k_1}\delta_{i_2k_2}, \quad (\hat{\mathrm{p}}_y^2)_{IK} = \delta_{i_1k_1}(\hat{\mathrm{p}}^2)_{i_2k_2} \quad (20)$$

with the matrices $(\hat{\mathrm{p}}^2)_{ik}$ taken from (16) with the obvious substitution of a, L, N by the corresponding quantities referring to the respective direction. Note that in more than one dimension many vanishing matrix elements appear in a typical Hamiltonian. One may thus consider to store it in a sparse matrix mode as a list of the nonvanishing elements rather than a full matrix.

The two-dimensional Henon-Heiles system is treated as an example in Sec. IV G and the MATLAB [22] code which generates the matrix representation of this two-dimensional problem is explicitly given in the appendix.

The algorithm is not time critical for the one-dimensional problems discussed in this paper, which means we find well converged results for these systems in less than a second on a modern standard computer. For the two-dimensional Henon-Heiles system, around 5 minutes are needed to find the eigenenergies and around 60 minutes are required to find the eigenfunctions in addition when using 101x101 points. Therefore, an implementation in programming languages like FORTRAN or C which would speed up the algorithm is a possible future option, but was not needed for the examples considered in this work. Furthermore, with only a single matrix diagonalization many bound states with eigenenergies E_n are found simultaneously. Other algorithms [10, 23] which were previously used to solve the one-dimensional Schrödinger equation with position-dependent masses consist of "guessing" an eigenenergy E and a subsequent test whether the resulting wave function has the correct behavior to fulfill the Schrödinger equation or not.

IV. EXAMPLE APPLICATIONS OF THE MATRIX ALGORITHM

A. The inversion motion of NH_3

To calculate the energy levels describing the inversion motion in ammonia with our algorithm, we exactly follow the procedure in [7] and first represent the data points (from table 1 in [7]) for the double-well potential $V(x)$ describing the inversion mode by an even polynomial of degree 20. Our coefficients are listed in the appendix. It might be noted that the potential obtained with DFT is in good agreement with the experimental value for the equilibrium geometry in [24] and the obtained barrier height of 2013.5 cm^{-1} agrees well with the one from empirical procedures (2018 $\pm$10 cm^{-1} [8]). In addition, the theoretical study in [8] yields an effective barrier height of 2021 $\pm$ 20 cm^{-1}. The potential is therefore very useful for a one-dimensional study, though the method is nevertheless a little bit questionable, because the theoretical effective barrier in [8] is only obtained, if one takes into account the zero-point vibrational energies of the other vibrational degrees of freedom, which adds a value of 244 $\pm$ 14 cm^{-1} to the barrier height according to [8].

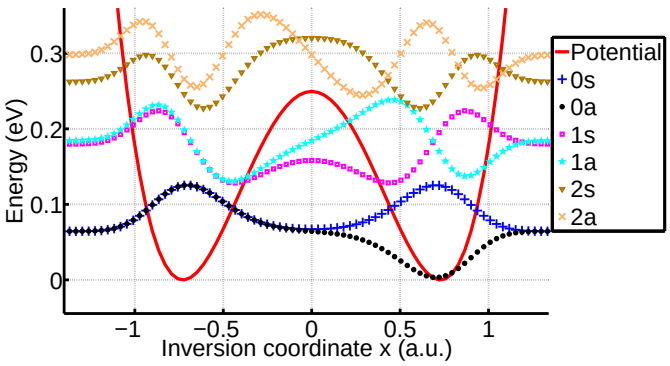

FIG. 1: (Color online) Potential curve (solid red line, data from [7]) and wave functions (symbols, see legend in the graph) of the 6 energetically lowest states 0s to 2a. The wave functions have been shifted by constants such that their values at $|x| \to \infty$ displays the eigenenergies. In the calculation, a width of $L = 4$ a.u. and $N = 111$ points were used.

The goal is now to solve the Schrödinger equation [37],

$$\Psi''(x) = 2\mu(x)\left[V(x) - E\right]\Psi(x), \quad (21)$$

or equivalently,

$$\left(\frac{1}{2\mu(x)}\hat{\mathrm{p}}^2 + V(x)\right)\Psi(x) = E\Psi(x) \quad (22)$$

with the position-dependent reduced mass

$$\mu(x) = \frac{3mM}{3m+M} + \frac{3mx^2}{r_0^2 - x^2}, \quad (23)$$

where m is the mass of a hydrogen atom, M the one of the nitrogen atom, and $r_0 = 1.00410198$ a. u. is given in [7] as the N-H distance which minimizes the energy of the molecule in planar geometry. The result of the matrix diagonalization is illustrated in Fig. 1 and the obtained energies are listed in Table I. The states are named using the symmetry label *symmetric* (s) or *antisymmetric* (a) together with an index n where $n = 0$ stands for the energetically lowest state with symmetric or antisymmetric character. Thus 0s designates the symmetric ground state and we give the other energies relative to this level. A comparison of the energy levels found with the matrix algorithm to the energy levels in table I of [7] shows perfect agreement.

As has been mentioned in Sec. II, the obtained eigenenergies should ideally not change drastically, if one puts the position-dependent mass into the Schrödinger equation in another form. Table II shows the eigenenergies obtained with Eqs. (3) to (6). We find a maximal relative deviation of the eigenenergies listed in Table I of about

State	μ=const [7]	Ref. [7]	This work	Experiment
0s	0.00	0.000	0.000	0.000
0a	1.05	0.837	0.837	0.793 [25]
1s	977.23	931.72	931.72	932.43 [26]
1a	1030.12	968.67	968.67	968.12 [26]
2s	1651.69	1596.76	1596.76	1598.47 [27]
2a	2011.44	1885.33	1885.33	1882.18 [27]
3s	2558.75	2389.14	2389.15	2384.17 [27]
3a	3142.66	2902.99	2902.99	2895.61 [27]

TABLE I: Inversion energy levels of NH_3 (shifted by E_{0s}) in cm^{-1}. The energies of our work were found with $L = 4.0$ a. u., $N = 111$ points and adopting the same 1D potential as in [7].

State	Eq. (3)	Eq. (4)	Eq. (5)	Eq. (6)
0s	0.000	0.000	0.000	0.000
0a	0.837	0.833	0.837	0.837
1s	931.71	932.01	931.72	931.72
1a	968.64	968.81	968.67	968.67
2s	1596.77	1597.36	1596.76	1596.76
2a	1885.25	1885.45	1885.33	1885.33
3s	2389.03	2389.21	2389.15	2389.15
3a	2902.82	2902.84	2902.99	2902.99

TABLE II: Inversion energy levels of NH_3 (shifted by E_{0s}) in cm^{-1} for different implementations of the position-dependent reduced mass. In the calculations $L = 4.0$ a. u. and $N = 111$ points were used.

0.5% (0.005 cm^{-1}) for the 0a state, indicating that the choice where to put the reduced mass has only a very minor influence on the resulting energies within the given accuracy.

B. Inversion energy levels of ND_3

In addition to NH_3, we test our algorithm by finding the energy levels of ND_3 which were not calculated in [7]. This is also of physical interest, since it is a further check of the adopted position-dependent mass model. Therefore, we simply replace the mass of the hydrogen atom by the mass of deuterium m_D=2.013553212712 amu [28] and solve the Schrödinger equation (5). The obtained energies are listed in Table III. It turns out that the inversion splitting can be reproduced and the energy levels for higher excited vibrational states have a relative error $\frac{|E_{calc}-E_{exp}|}{E_{exp}} \leq 0.7\%$ in comparison to the experiment whereas the use of the constant reduced mass

$$\mu = \frac{3mM}{3m+M}\left(1+\frac{3m\sin^2\beta_e}{M}\right) \qquad (24)$$

from [29] with $\beta_e = 22°13'$ (from [7]) leads to higher energy values and, therefore, larger relative errors (up to

State	This work μ=const Eq. (24)	This work $\mu(x)$ Eq. (23)	Experiment [25]
0s	0	0	0
0a	0.05	0.05	0.05
1s	793.8	746.2	745.6
1a	798.3	749.3	749.15
2s	1419.7	1368.4	1359.0
2a	1513.7	1432.0	1429.0
3s	1912.6	1836.4	1830.0
3a	2238.4	2106.4	2106.6

TABLE III: Inversion energy levels of ND_3 (shifted by E_{0s}) in cm^{-1}. The calculations were done with $L = 4.0$ a.u. and $N = 111$ points.

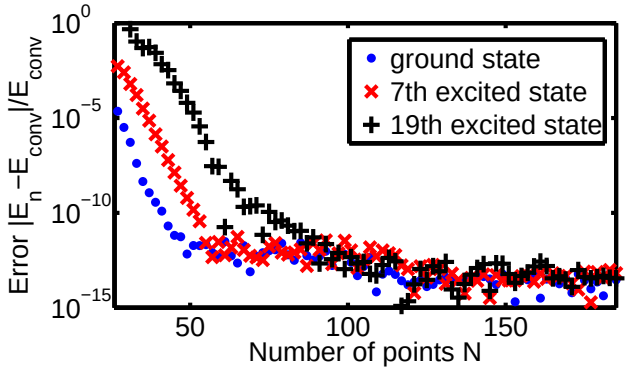

FIG. 2: (Color online) Convergence behavior with respect to a variation of the lattice spacing that is proportional to $1/N$ as we hold fixed the width $L = 4.5$ a. u. We show the ground state and the 7th as well as the 19th excited state. Relative errors of the energies $\frac{|E_n-E_{conv}|}{E_{conv}}$ are plotted, where E_{conv} is the 'converged' energy (average over the 10 largest N-values).

6.6%). Even though the agreement with the experiment is very good, it still has to be noted that according to [8] the barrier height depends on the zero-point vibrational energy of the other vibrational degrees of freedom, and this zero-point vibrational energy depends on the isotope.

C. Convergence properties

We discuss the convergence behavior of the matrix algorithm on the example of NH_3 (Sec. IV A). We use Eq. (4) as Hamiltonian and the number of points N is varied first for fixed $L = 4.5$ a. u. with the result shown in Fig. 2. In this way the dependence on the resolution given by the lattice spacing was tested. In Fig. 3 we have frozen the spacing to $a = 4.5/151$ a. u. and thus test stability when changing L. The nearly straight lines in the semilogarithmic plot indicate exponential convergence behavior with respect to both regulators.

The convergence that we have demonstrated in our

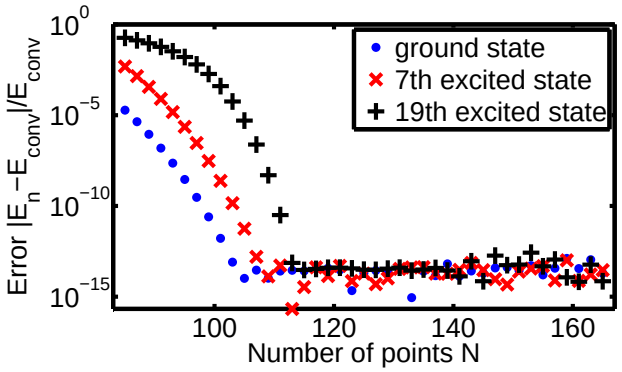

FIG. 3: (Color online) as Fig. 2, but now $a = 4.5/151$ a. u. is fixed and thus L varies proportional to the number of points N.

first test is actually physically plausible. As indicated before the only exponentially small sensitivity with respect to (large) L is due to the smallness of the wave functions for bound states deep in the classically forbidden region. The same wave functions in momentum space will also have an exponential fall-off at large momenta so that a dual argument holds in momentum space. We may argue here by analogy with the sampling theorem [30]. A continuous time signal that contains no frequencies beyond the Nyquist frequency $\omega = \pi/\tau$ can be *exactly* reconstructed from sampling it at discrete times separated by τ (CD player). In analogy, if the support of our bound state wave functions would be *exactly* contained in the interval $[-\pi/a, \pi/a]$ then the *exact* wave function for continuous x could be reconstructed form the Fourier components (discrete and finite in number for finite L). Then there obviously is an exact correspondence between derivatives d/dx and factors ip. In reality the boundstates do not have compact momentum support, but the deviation is only caused by the exponentially small tales for small enough a.

D. Morse potential

The discrete position (momentum) space introduced in the matrix algorithm is symmetric with respect to $x = 0$ ($p = 0$) as is also the double-well problem discussed in the previous section. Nevertheless, general Hamiltonians can be non-symmetric and may also have a partially continuous spectrum (in the infinite volume). Therefore we want to investigate, if bound states can still be found accurately and efficiently using the matrix algorithm also in this more general case. A popular example for a non-symmetric potential with bound and continuum states is the Morse potential

$$V(R) = D_e \left(1 - e^{-\alpha(R-R_e)}\right)^2 . \tag{25}$$

Often the vibration of a diatomic molecule can be well-described by this potential. The energy spectrum for the bound states of this potential is known analytically [31],

$$E_n = 2\pi\hbar\nu_0 \left(n + \frac{1}{2}\right) - \frac{\pi^2\hbar^2\nu_0^2}{D_e}\left(n + \frac{1}{2}\right)^2 , \tag{26}$$

with $\nu_0 = \frac{\alpha}{2\pi}\sqrt{\frac{2D_e}{\mu}}$ where μ is (again) the reduced mass. We investigate a Morse potential with parameters $D_e = \mu = 1$ and $\alpha = 0.24$, $R_e = -35$ where 6 vibrational bound states exist. Table IV shows the energies obtained by the matrix algorithm with $N = 111$ points and $L = 90$ together with the exact results from Eq. (26). We still find excellent agreement except for some visible discrepancy for the highest lying 6th vibrational state. This can be understood, since states close to the continuum are more extended in space. If $N = 201$ points, $L = 140$, and $R_e = -60$ are used, all eigenenergies obtained by the matrix algorithm are identical to the analytical results within the accuracy given in Table IV.

In addition to the bound states, we obtain discretized continuum states on which the periodic boundary conditions of the method are imprinted. To check whether this discretized continuum can approximately represent the true continuum, we examined as an example the relation

$$\langle 0|\hat{x}^2|0\rangle \approx \sum_{n=0}^{n_{\max}} \langle 0|\hat{x}|n\rangle \langle n|\hat{x}|0\rangle \tag{27}$$

using the discretized states $|n\rangle$. Using $N = 301$ points, $L = 140$, and $R_e = -60$ the relative error

$$\epsilon(n_{\max}) = \frac{\left|\langle 0|\hat{x}^2|0\rangle - \sum_{n=0}^{n_{\max}} \langle 0|\hat{x}|n\rangle \langle n|\hat{x}|0\rangle\right|}{\langle 0|\hat{x}^2|0\rangle} \tag{28}$$

was calculated. With a restriction of the summation to bound states only we find $\epsilon(n_{\max} = 5) \approx 10^{-6}$. When we further increase $n_{\max}$ the error decreases monotonically until machine precision is reached ($\epsilon(n_{\max}) < 10^{-14}$ for $n_{\max} > 116$). Thus the completeness relation of the eigenstates is numerically fulfilled, if also the discretized continuum states are considered. We conclude that any upcoming non-symmetric problem that contains a continuum spectrum should also be well treatable by the matrix algorithm, if discretized continuum states (with periodic boundary conditions) are sufficient as is the case in the here considered example of bound to continuum transitions.

E. Harmonic oscillator with a position-dependent mass

To compare the present matrix algorithm to the recently published traditional second-order Hartree shoot-

n	Matrix algorithm	Exact
0	0.1625056275	0.1625056275
1	0.4443168825	0.4443168825
2	0.6685281374	0.6685281374
3	0.8351393923	0.8351393924
4	0.9441506473	0.9441506474
5	0.9955620565	0.9955619023

TABLE IV: Eigenenergies of the Morse potential (25) obtained with $N = 111$ points and $L = 90$ for the model parameters $D_e = \hbar = \mu = 1$ and $\alpha = 0.24$, $R_e = -35$. The exact values were obtained using Eq. (26).

ing method [10], we implemented the two model Hamiltonians

$$\hat{\mathrm{H}}_1 = \frac{1}{2}\ \hat{\mathrm{p}}\ \frac{1}{1+\hat{\mathrm{x}}^2}\ \hat{\mathrm{p}} + \frac{1}{2}\ \hat{\mathrm{x}}^2 \tag{29}$$

and

$$\hat{\mathrm{H}}_2 = \frac{1}{2}\ \hat{\mathrm{p}} \left(\frac{1+\hat{\mathrm{x}}^2}{2+\hat{\mathrm{x}}^2}\right)^2 \hat{\mathrm{p}} + \frac{1}{2}\ \hat{\mathrm{x}}^2. \tag{30}$$

When we compare our eigenenergies obtained by the matrix algorithm with $N = 201$ points and $L = 20$ (which is well within the converged regime), we reproduce table 1 (for $\hat{\mathrm{H}}_1$) and table 3 (for $\hat{\mathrm{H}}_2$) in [10] to all digits. Considering the convergence properties, qualitatively the same exponential behavior is found as shown in Figs. 2 and 3. One should note that the second-order shooting method in [10] only converges quadratically and, therefore, much larger numbers of evenly spaced points ($N = 640, 960, 1440$ and 2160) were needed to obtain the results.

F. Non-Hermitian PT-symmetric and non-symmetric cases

As mentioned in Sec. II, the PT-symmetric Hamiltonians examined in Sec. II and IV A are rather special. Therefore, we will briefly discuss the more usual form of a PT-symmetric Hamiltonian with a constant mass but a complex potential. We want to demonstrate that the matrix algorithm is also applicable for such types of problems, since complex matrices can also be treated. Therefore, we implemented the model Hamiltonian

$$\hat{\mathrm{H}} = \hat{\mathrm{p}}^2 + \hat{\mathrm{x}}^2 + i\ \hat{\mathrm{x}}. \tag{31}$$

According to [12], this PT-symmetric Hamiltonian has the real eigenenergies

$$E_n = 2\ n + \frac{5}{4}. \tag{32}$$

In contrast, the non-Hermitian and not PT-symmetric Hamiltonian

$$\hat{\mathrm{H}} = \hat{\mathrm{p}}^2 + \hat{\mathrm{x}}^2 + i\ \hat{\mathrm{x}} - \hat{\mathrm{x}} \tag{33}$$

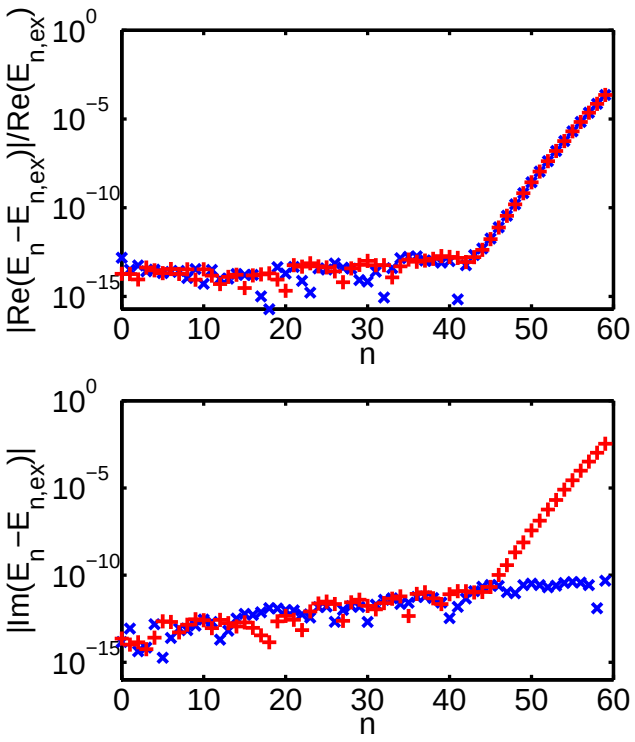

FIG. 4: (Color online) **Top**: Relative Error of the real part of the eigenvalues of Eqs. (31) [x] and (33) [+]. The values were obtained with the matrix algorithm using $N = 101$ points and $L = 25$. The exact values $E_{n,\mathrm{ex}}$ are given by Eqs. (32) and (34).
Bottom: Absolute Error of the imaginary part of the eigenvalues (same L and N).

has according to [12] the complex eigenvalues

$$E_n = 2\ n + 1 + \frac{1}{2}\ i \tag{34}$$

which can no longer be interpreted as eigenenergies. The relative error of the real part as well as the absolute error of the imaginary part of the eigenvalues obtained with the matrix algorithm with $N = 101$ points and $L = 25$ is shown in Fig. 4. The eigenvalues of the Hamiltonian in Eq. (31) now contain a small imaginary part (also see Fig. 4) due to roundoff errors which was not the case for the PT-symmetric Hamiltonians in Eqs. (5) and (6). The reason is that the matrix representations of Eqs. (5) and (6) are real, while the matrix representation of Eq. (31) is complex. Nevertheless, the very good agreement of our results with Eqs. (32) and (34) (relative error below 10^{-12} for $n < 45$) shows that our matrix algorithm can also be very helpful to find eigenenergies of PT-symmetric Hamiltonians. In critical cases one could in principle consider increasing the numerical precision (either in steps from single to quadruple precision or, even better, digit-by-digit) to probe further whether the eigenvalue spectrum is purely real or not.

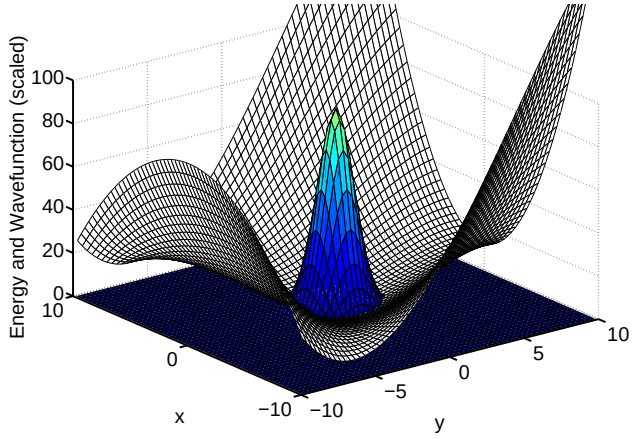

FIG. 5: (Color online) Potential energy surface (filled white) and obtained (discrete) ground state wavefunction (filled blue, scaled arbitrary) of the Henon-Heiles system in Eq. (35) with $\lambda = 1/\sqrt{80}$. A $L_x \times L_y = 20 \times 20$ grid with $N_x \times N_y = 61 \times 61$ points was used.

G. The two-dimensional Henon-Heiles system

To demonstrate the performance of the matrix algorithm in two dimensions we investigate the Henon-Heiles system [32]

$$\hat{\mathrm{H}} = \frac{1}{2}\left(\hat{\mathrm{p}}_x^2 + \hat{\mathrm{p}}_y^2\right) + \frac{1}{2}\left(\hat{\mathrm{x}}^2 + \hat{\mathrm{y}}^2\right) + \lambda\left(\hat{\mathrm{x}}^2\,\hat{\mathrm{y}} - \frac{\hat{\mathrm{y}}^3}{3}\right). \quad (35)$$

This model potential is frequently used as a benchmark for numerical methods [33–35], although the potential in Eq. (35) is not bounded from below and thus it does not support true bound states but only metastable ones that decay by tunneling through the barriers as is discussed in, e. g., Refs. [35, 36]. We use $\lambda = 1/\sqrt{80}$ to compare our lowest 36 eigenenergies with the ones obtained in [35]. The MATLAB [22] program which generates the matrix representation of Eq. (35) is given in the appendix. When using a $L_x \times L_y = 20 \times 20$ grid with $N_x \times N_y = 61 \times 61$ points, we reproduce all 36 eigenenergies given in [35] within the given accuracy. The obtained ground state wavefunction is shown together with the potential in Fig. 5. When increasing the number of grid points to $N_x \times N_y = 81 \times 81$ and $N_x \times N_y = 101 \times 101$ ($L_x \times L_y = 20 \times 20$ held constant) or changing the grid size to $L_x \times L_y = 18 \times 18$ and $L_x \times L_y = 22 \times 22$ ($a_x = a_y = 20/61$ approximately held constant), the obtained energies are stable within an accuracy of at least 12 significant digits [38]. Thus the matrix algorithm is also very suitable for finding bound states of two-dimensional Hamiltonians.

V. SUMMARY

The matrix algorithm presented in this paper is easy to implement, flexible, and shows exponential convergence (with respect to the number of grid points N and width L). While other algorithms [10, 23] usually consist of guessing an initial energy, this algorithm represents a much more direct method, since one finds a set of eigenenergies by just a single matrix diagonalization. To demonstrate the performance of the algorithm it was applied to a one-dimensional model describing the inversion motion of NH_3 and ND_3. Furthermore, different forms for the position-dependent mass Hamiltonian were discussed. A great advantage is the flexibility of the present algorithm to handle their different possible forms. Especially, it is possible to avoid non-Hermitian model Hamiltonians (as used for, e. g., describing inversion of NH_3) that are often only adopted, because the symmetrized Hermitian form of the Hamiltonian leads to a Schrödinger equation that cannot be solved with many of the standard numerical algorithms.

In the case of ammonia it turns out that the eigenenergies do not strongly depend on the choice where one puts the mass into the Hamiltonian. This justifies the underlying classical derivation of the model Hamiltonian with a position-dependent mass. Also the eigenenergies of a Morse potential were determined. The results indicate that the algorithm is applicable to find bound states of general Hamiltonians that may contain asymmetric potentials and include a continuous spectrum. The algorithm was also successfully applied to non-Hermitian Hamiltonians both with or without PT symmetry. This allows to numerically check whether the eigenvalue spectrum of such an Hamiltonian is purely real or not and demonstrates that the algorithm can handle Schrödinger equations with complex eigenvalue spectra. Finally, it was demonstrated with the aid of a two-dimensional problem that the algorithm is straightforwardly applied to higher-dimensional problems, only limited by the increasing numerical efforts due to the exploding number of grid points needed.

For very large problems or to go beyond two dimensions it may be useful to write a routine that applies $\hat{\mathrm{H}}$ to a vector Ψ and renounce at storing any matrix at all. Such a routine would apply FFT twice for each direction in every call with the cost scaling like $N^D \ln N$. If only some low-lying energies are requested, the use of a Lanczos- or Arnoldi-type algorithm would be a natural choice for enhancing the efficiency. Within Matlab the eigenvalue finder `eigs` would allow for such an approach and `fft` is available as well.

Acknowledgments

We thank Dr. Oliver Bär for helpful discussions.

Appendix A: Matlab code fragments

The following short MATLAB [22] function generates the lattice and the real antisymmetric matrix $i\hat{p}$ for given integer M and width L that will enter into the construction of Hamiltonians:

```
function [x,ip_op] = gen_mommatrix(L,M)
% generate the lattice x      (vector)
% and i times p-operator (real,antisymmetric)
%
N=2*M+1;
a=L/N;                % spacing
x=a*(-M:M);           % x-values
ip_op=zeros(N,N);     % matrix p
c1=pi/L;
c2=pi*(N+1)/N;
for i=1:N-1
  for k=i+1:N
      ip_op(i,k)=c1/sin(c2*(i-k));
      ip_op(k,i)=-ip_op(i,k);
  end
end
```

For the ammonia inversion problem the following constants are required:

```
%constants from \protect\vrule width0pt\protect\href{http://physics.nist.gov/cuu/}{http://physics.nist.gov/cuu/}
Hartreecm=219474.63137;%1 a.u. (Hartree energy)
                       %in 1/cm
aBohr=0.52917721092;   %1 a.u. (Bohr radius)
                       %in Angstrom
%constants from ref. Aquino et al.
m=1.007825035;      %hydrogen mass in amu
%m=2.013553212712;  %deuterium mass in amu (from nist)
M=14.003074;        %nitrogen mass in amu
amu=1822.888;       %1 amu in a.u.
r0=1.00410198/aBohr;%N-H-distance in a.u.
% Potential fit parameters:
%V=sum_{i=0}^{i=10} K(i+1) x_^{2i}
% [x in Angstrom, V in a.u.]
K=[ 0                ...
-1.2760373471398e-01 ...
 4.7973549262032e-01 ...
-4.4967805753691e-01 ...
 3.4048981035460e+00 ...
-2.5268066877745e+01 ...
 1.1565093681631e+02 ...
-3.2323821164423e+02 ...
 5.4331165379878e+02 ...
-5.0630533518111e+02 ...
 2.0128292638493e+02 ];
```

The Hamiltonian is constructed by the following sequence of steps (for $L = 4, N = 111$):

```
[x,ip_op] = gen_mommatrix(4,55);
% x-dependent mass
mux=3*m*M/(3*m+M)+3*m*x.^2./(r0^2-x.^2);
mux=mux*amu; % conversion amu -> a.u.
% kinetic part
psq=-ip_op^2;
H=-0.5*ip_op*diag(1./mux)*ip_op;            %Eq.(3)
%H=0.25*(diag(1./mux)*psq+psq*diag(1./mux));%Eq.(4)
%H=0.5*diag(1./mux)*psq;                    %Eq.(5)
%H=0.5*psq*diag(1./mux);                    %Eq.(6)

% add potential part
Vpot=polyval(fliplr(K),(x*aBohr).^2); % evaluate
                                      % polynomial
H=H+diag(Vpot);
```

Eigenenergies and eigenfunctions can now be found using:

```
[V,En]=eig(H);
```

The following MATLAB [22] program generates the matrix representation for the two-dimensional Henon-Heiles system (35) using $N_x = N_y = N = 2M + 1$ points with $L_x = L_y = L$:

```
[x,ip_op] = gen_mommatrix(L,M);
psq=-ip_op^2;
del=eye(2*M+1); % unit matrix
H=0.5*(kron(psq,del)+kron(del,psq)+...
   kron(diag(x.^2),del)+kron(del,diag(x.^2)))+...
   (1/sqrt(80))*(kron(diag(x.^2),diag(x))-...
   kron(del,diag(x.^3))/3);
```

We have used the MATLAB function `kron` that builds the tensor (Kronecker) product of two matrices. The generalization to discretizations that are anisotropic in x and y and also to more than two dimensions is obvious, and eigenvalues of $\hat{\mathrm{H}}$ are found as before.

[1] G. Levai and O. Özer, J. Math. Phys. **51**, 092103 (2010).
[2] G. Bastard, *Wave Mechanics Applied to Semiconductor Heterostructures* (Les Editions de Physique, Les Ulis, 1988).
[3] M. Barranco, M. Pi, S. Gatica, E. Hernandez, and J. Navarro, Phys. Rev. B **56**, 8997 (1997).
[4] G. Bastard, Phys. Rev. B **24**, 5693 (1981).
[5] M. Manning, J. Chem. Phys. **3**, 136 (1935).
[6] D. Rush and K. Wiberg, J. Phys. Chem. A **101**, 3143 (1997).
[7] N. Aquino, G. Campoy, and H. Yee-Madeira, Chem. Phys. Lett. **296**, 111 (1998).
[8] W. Klopper, C. Samson, G. Tarczay, and A. Csaszar, J. Comp. Chem. **22**, 1306 (2001).
[9] J. Gordon, H. Zeiger, and C. Townes, Phys. Rev. **95**, 282 (1954).
[10] J. Killingbeck, J. Phys. A **44**, 285208 (2011).
[11] P. Jha, H. Eleuch, and Y. Rostovtsev, J. Mod. Opt. **58**, 652 (2011).
[12] C. Bender and S. Boettcher, Phys. Rev. Lett. **80**, 5243 (1998).
[13] A. Mostafazadeh, J. Math. Phys. **43**, 205 (2002).
[14] A. Saenz, J. Phys. B **33**, 4365 (2000).
[15] E. Goll, G. Wunner, and A. Saenz, Phys. Rev. Lett. **97**, 103003 (2006).
[16] O. von Roos, Phys. Rev. B **27**, 7547 (1983).

[17] J. Cooley, **15**, 363 (1961).
[18] B. Johnson, J. Chem. Phys. **67**, 4086 (1977).
[19] C. Wozar and A. Wipf, Ann. of Phys. **327**, 774 (2012).
[20] S. D. Drell, M. Weinstein, and S. Yankielowicz, Phys. Rev. **D14**, 1627 (1976).
[21] L. H. Karsten and J. Smit, Phys. Lett. **B85**, 100 (1979).
[22] *Matlab*, http://www.mathworks.com/products/matlab/.
[23] J. Rivas-Silva, G. Campoy, and A. Palma, Int. J. Quant. Chem. **40**, 405 (1991).
[24] J. Swalen and J. Ibers, J. Chem. Phys. **36**, 1914 (1962).
[25] V. Spirko, J. Mol. Spectrosc. **101**, 30 (1983).
[26] W. Gordy and R. Cook, *Microwave Molecular Spectra* (Interscience, New York, 1970).
[27] S. Urban, V. Spirko, D. Papousek, J. Kauppinen, S. Belov, L. Gershtein, and A. Krupnov, J. Mol. Spectrosc. **88**, 274 (1981).
[28] http://physics.nist.gov/cuu/.
[29] C. Townes and A. Shalow, *Microwave Spectroscopy* (Dover, New York, 1975).
[30] W. H. Press, B. P. Flannery, S. A. Teukolsky, and W. T. Vetterling, *Numerical Recipes: The Art of Scientific Computing* (Cambridge Univ. Press, Cambridge, 1986).
[31] P. Morse, Phys. Rev. **34**, 57 (1929).
[32] M. Henon and C. Heiles, Astronom. J. **69**, 73 (1964).
[33] J. Ehave and D. C. Clary, Chem. Phys. Lett. **190**, 225 (1992).
[34] D. S. Zhang, G. W. Wei, D. J. Kouri, and D. K. Hoffman, J. Chem. Phys. **106**, 5216 (1997).
[35] B. Poirier and J. C. Light, J. Chem. Phys. **111**, 4869 (1999).
[36] B. A. Waite and W. H. Miller, J. Chem. Phys. **74**, 3910 (1981).
[37] Unless otherwise noted, we work in atomic units with $\hbar = m_e = e^2 = 4\pi\epsilon_0 = 1$ which also puts a_{Bohr} and E_{Hartree} to unity. To conform with the literature we convert some energies to 1/cm and lengths to Å. Conversion constants can be found in the appendix.
[38] For the larger grid with $L_x \times L_y = 22 \times 22$ one additional state appears within the lowest 37 eigenenergies that is ignored in the comparison since its energy depends on the box size. This state is localized outside the potential well and its appearance is a consequence of the mentioned fact that the Henon-Heiles potential is not bounded from below.